Title

New Insights on the Structure of Electrochemically Deposited Lithium Metal and Its Solid Electrolyte Interphases via Cryogenic TEM.

Journal

Nano letters, 17(12)

ISSN

1530-6984

Authors

Wang, Xuefeng
Zhang, Minghao
Alvarado, Judith
et al.

Publication Date

2017-12-01

DOI

10.1021/acs.nanolett.7b03606

Peer reviewed

NANO LETTERS
Cite This: Nano Lett. XXXX, XXX, XXX-XXX
Letter
pubs.acs.org/NanoLett

New Insights on the Structure of Electrochemically Deposited Lithium Metal and Its Solid Electrolyte Interphases via Cryogenic TEM

Xuefeng Wang,[†] Minghao Zhang,[†,§] Judith Alvarado,[†,§] Shen Wang,[†] Mahsa Sina,[†] Bingyu Lu,[†] James Bouwer,[‡] Wu Xu,[∥] Jie Xiao,[∥] Ji-Guang Zhang,[∥] Jun Liu,[∥] and Ying Shirley Meng*[,†,§]

[†]Department of NanoEngineering, [‡]Department of Chemistry and Biochemistry, and [§]Materials Science and Engineering, University of California San Diego, 9500 Gilman Drive, La Jolla, California 92093, United States

[∥]Energy and Environmental Directorate, Pacific Northwest National Laboratory, 902 Battelle Boulevard, Richland, Washington 99354, United States

Supporting Information

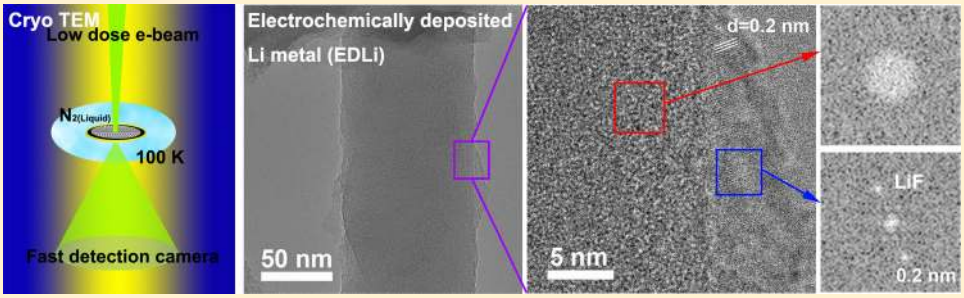

ABSTRACT: Lithium metal has been considered the "holy grail" anode material for rechargeable batteries despite the fact that its dendritic growth and low Coulombic efficiency (CE) have crippled its practical use for decades. Its high chemical reactivity and low stability make it difficult to explore the intrinsic chemical and physical properties of the electrochemically deposited lithium (EDLi) and its accompanying solid electrolyte interphase (SEI). To prevent the dendritic growth and enhance the electrochemical reversibility, it is crucial to understand the nano- and mesostructures of EDLi. However, Li metal is very sensitive to beam damage and has low contrast for commonly used characterization techniques such as electron microscopy. Inspired by biological imaging techniques, this work demonstrates the power of cryogenic (cryo)-electron microscopy to reveal the detailed structure of EDLi and the SEI composition at the nanoscale while minimizing beam damage during imaging. Surprisingly, the results show that the nucleation-dominated EDLi (5 min at 0.5 mA cm^{-2}) is amorphous, while there is some crystalline LiF present in the SEI. The EDLi grown from various electrolytes with different additives exhibits distinctive surface properties. Consequently, these results highlight the importance of the SEI and its relationship with the CE. Our findings not only illustrate the capabilities of cryogenic microscopy for beam (thermal)-sensitive materials but also yield crucial structural information on the EDLi evolution with and without electrolyte additives.

KEYWORDS: *Li metal, electrochemical deposition, SEI, cryogenic TEM*

Lithium (Li) metal is the most attractive anode material for rechargeable batteries due to its low electrode potential (−3.04 V versus a standard hydrogen electrode) and high theoretical specific capacity (3860 mAh g^{-1}) compared with the present electrode materials.[1,2] The use of Li metal as an anode dates back to the early Li batteries with TiS_2 as the cathode (Figure 1);[3] however, the aggressive dendritic growth of Li metal during cycling makes it too dangerous for practical use. To combat these issues, the high capacity of the current commercial Li-ion batteries was sacrificed by the use of Li-intercalated compounds (graphite (372 mAh g^{-1}) as the anode and layered oxides (e.g., $LiCoO_2$) as the cathode).[4,5] Nevertheless, an increased demand for higher energy density batteries requires a breakthrough in the safety and long-term cycling stability of Li metal anode to enable the practical application of high-energy Li metal batteries that use either conversion reaction materials such as sulfur (S, 2567 Wh kg^{-1}) and oxygen (O_2, 3505 Wh kg^{-1}) or using Li intercalation compounds (such as $LiNi_{0.8}Mn_{0.1}Co_{0.1}O_2$) as cathodes.[6]

However, several challenges that have persisted from the 1960s must be addressed to facilitate the next generation high-energy density battery systems, such as preventing the formation of Li metal dendrites and alleviating the high reactivity with electrolyte that forms the solid electrolyte interphase (SEI).[7−11] A prerequisite to solve these issues is to

Received: August 22, 2017
Revised: October 28, 2017
Published: November 1, 2017

DOI: 10.1021/acs.nanolett.7b03606
Nano Lett. XXXX, XXX, XXX−XXX

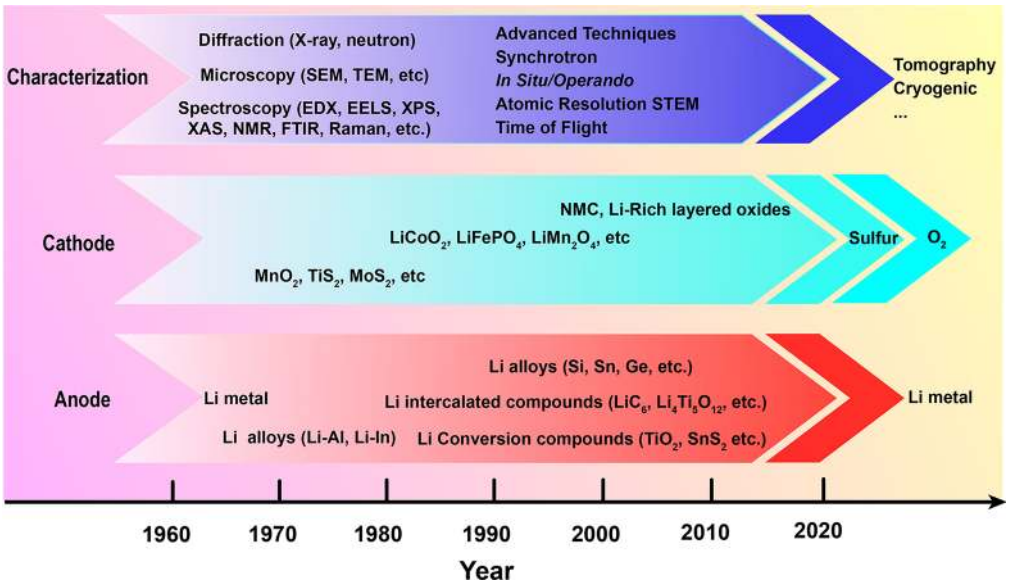

Figure 1. Timeline development of the Li batteries in terms of anode, cathode, and characterization techniques used to understand mechanisms. (SEM: scanning electron microscope; TEM: transmission electron microscopy; EDX: energy-dispersive X-ray spectroscopy; EELS: electron energy loss spectroscopy; XPS: X-ray photoelectron spectroscopy; FTIR: Fourier transform infrared spectroscopy; XAS: X-ray adsorption spectroscopy; NMR: nuclear magnetic resonance; STEM: scanning transmission electron microscopy; and NMC: lithium nickel manganese cobalt oxides.).

understand the properties, nanostructures, and growth mechanism of the electrochemically deposited Li metal (EDLi). Although various characterization techniques have been developed in the Li battery research field (Figure 1),[23] some of them fail to properly characterize Li metal because the intrinsic high chemical reactivity and low thermal stability make it difficult to handle the sample without damaging or contaminating. This is evident when observing Li metal by conventional transmission electron microscopy (TEM), with which severe beam damage occurs after short exposure time (seconds), which is demonstrated and discussed later in this work. Currently, researchers have attempted to uncover the Li metal growth process by in situ microscopy, optical microscopy,[12,13] scanning electron microscopy (SEM),[14] and atomic force microscopy (AFM).[15,16] The above-mentioned techniques demonstrate that the Li dendrites first nucleate, then propagate unevenly and intrusively throughout the current collector. Synchrotron hard X-ray microtomography further exhibited a three-dimensional loose and interwoven microstructure of EDLi film. The chemical composition of the SEI is commonly investigated by X-ray photoelectron spectroscopy (XPS) and Fourier transform infrared spectroscopy (FTIR);[17,18] however, its distribution on the surface of the Li metal is unknown because the generated signal comes from the average sample area. Note that currently most of the above-mentioned techniques are limited to microscale spatial imaging and spectroscopy, while the detailed nanostructure of EDLi is not well-explored. Furthermore, its chemical composition and physical properties are not fully understood, which urgently calls researchers to develop novel tools to enable imaging techniques with high spatial resolution and spectroscopy techniques.

Cryogenic-electron microscopy (cryo-EM) has emerged over the past two decades as a structural biology characterization technique. It has achieved great success in determining the configuration of various proteins, ribonucleic acids, and other macromolecules.[19−22] The cryo-protection of the frozen biological samples allows the preservation of the intrinsic structural features. Recent advances in instrumentation and software renders high-resolution images under low-dose condition (<100 electons Angsrom^{-2} (e Å^{-2})).[23] To load the challenging vitrified ice samples, special loading devices were developed with a multispecimen cryo-holder (six TEM grids), a covered cryogenic dewar, and a vacuum-transfer device (Figure S1). The samples are viewed at low temperature (100 K) and under low-dose conditions (<100 e Å^{-2}) by the advanced complementary metal-oxide semiconductor-based direct detection detectors at a rate of 30 frames per second. As a result, biology researchers are able to align, drift-correct, and sum frames over many seconds with unprecedented resolution while maintaining high signal-to-noise ratio images under low-dose conditions.[24,25]

Borrowing techniques from the cryo-EM community, cryo-TEM can potentially be a powerful technique to image beam-sensitive battery electrode materials (Figure 1). Herein, we extend the use of cryo-TEM to Li metal using a Gatan 626 cryo-holder to cool the samples to approximately 100 K. This technique shows great promise in mitigating beam damage and producing high-resolution images. The challenges of imaging Li metal with TEM mirrors the challenges that biochemists faced when viewing frozen vitrified ice embedded proteins, which were addressed by using cryo-EM system. Cryo-EM outperforms other techniques used to characterize EDLi, with its ultrahigh resolution that allows us to detect the morphology and structure as well as the chemical composition and spatial distribution of the SEI on EDLi at the nano scale. For the first time, cryo-TEM elucidates the nanostructure of the EDLi and its surface film. Furthermore, distinctive surface layers are constructed by adding functional cesium ion (Cs^+) and zinc (Zn^{2+}) additives, and their relationships with the Coulombic efficiency (CE) are analyzed. Our findings demonstrate the power of cryo-TEM for beam-sensitive battery materials and provide new perspectives on (1) the structure of the EDLi and the SEI, (2) the effects of metal ions as electrolyte additives on the EDLi morphology, and (3) the relationship between the SEI and the CE.

DOI: 10.1021/acs.nanolett.7b03606
Nano Lett. XXXX, XXX, XXX−XXX

Feasibility of Cryo-TEM. Figure 2a shows the cell configuration of Li metal deposition for TEM, in which a

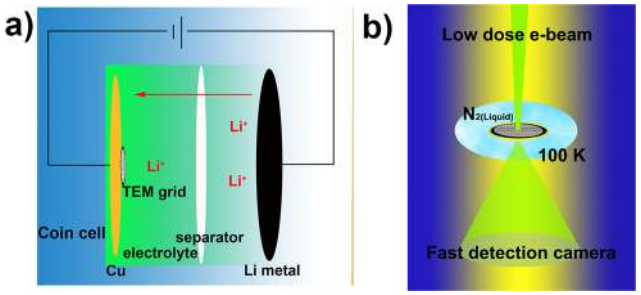

Figure 2. (a) Schematic cell configuration and (b) schematic cryo-TEM imaging of the EDLi for TEM observation.

grid (lacey carbon) was placed above the Cu foil on the cathode side and used as a part of the substrate with conventional carbonate electrolyte (1 mol L^{-1} lithium hexafluorophosphate ($LiPF_6$) in ethylene carbonate/ethyl methyl carbonate (EC/EMC, 50:50 wt %) with the moisture content of 22 ppm, BASF). As shown in Figure S1a, the Li metal deposits below 0.0 V at 0.5 mA cm^{-2}. The EDLi on the TEM grid (Figure S1b) has identical morphology to that deposited on the Cu foil (Figure S1c). A 5 min deposition was carried out to highlight the nucleation process. If the deposition process time was extended, the EDLi would completely cover the TEM grid making it unsuitable for TEM imaging. After deposition, the cell was disassembled in the glovebox where the grid was taken out and slightly rinsed with dimethyl carbonate (DMC) to remove trace electrolyte. The grids were then loaded in a covered cryogenic dewar with continuous Ar flow (system pictures in Figure S2). The holder was pumped down to 10^{-5} bar and quickly loaded into a vacuum-transfer chamber, where it remained under vacuum to be cooled to 100 K before introducing it to the microscope for viewing (Figure 2b at 100 K and under low-dose conditions (<100 e $Å^{-2}$)). This process minimizes the potential damage and contamination during sample transfer, guaranteeing that our results are trustworthy and reproducible.

Figure 3 compares the stability of the Li metal as a function of the electron radiation dose at room temperature (RT, 300 K) and low temperature (100 K). The EDLi shows a ribbon-like morphology with approximately 200−300 nm in diameter and a few micrometers in length (Figures 3 and S3). At 300 K, the EDLi is quite unstable even at a low magnification (19 000×) with about 8 e/$Å^2$ dose per image. It quickly drifted once the beam focused on the sample (Figure 3a), evaporated to form defects (Figure 3b, labeled with red arrow), and finally turned wholly molten (Figure 3c). In contrast, at 100 K, the EDLi is very stable (Figure 3d−f), and no visible changes were observed with the same dose conducted at RT. Enlarging the magnification will increase the radiation dose on each record. For example, at the 400 000× magnification, the radiation dose reaches 70 e $Å^{-2}$ per image (Figure 3g), which has a sufficiently high spatial resolution (~2 Å) to detect the lattice structural features. In this circumstance, the EDLi is still stable for at least 210 e $Å^{-2}$ (Figure 3g−i). Therefore, the cryo-TEM allows us to detect the EDLi at the nanoscale while avoiding beam damage.

The nanostructure of the EDLi is shown in Figure 4a. The identical contrast in the bulk demonstrates the uniformity of the EDLi. Along the edges of the EDLi an uneven SEI is

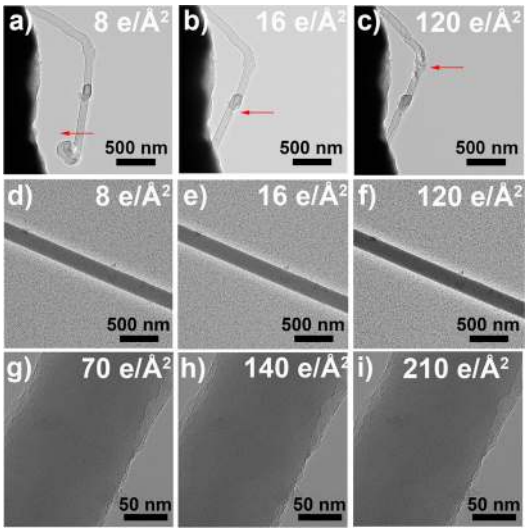

Figure 3. TEM images of the EDLi as a function of the electron radiation dose at 300 K (panels a−c at 19 000× magnification) and 100 K (panels d−f at 19 000× and panels g−i at 400 000× magnification).

present with a maximum thickness of ~7 nm. Figure 4b surprisingly displays lattice fringes present on the surface rather than the bulk, suggesting that the EDLi metal is amorphous while part of the SEI is crystalline. The above results were validated by the area fast Fourier transform (FFT) patterns. The absence of characteristic bright rings and spots in the bulk area (red square) ensures that the EDLi is amorphous (Figures 4b and S4). Conversely, two obvious characteristic bright spots appear at the SEI surface (blue square). The ~0.2 nm lattice spacing is consistent with the lattice plane distance of the LiF (200) and cannot be ascribed to any plane distance of the metallic Li (Table S1), further validating the partially crystallized SEI. The presence of the crystalline LiF in the SEI is also evidenced by the synchrotron X-ray scattering conducted by Bedzyk and co-workers.[26]

To find the influence of low temperature on the Li metal crystallinity, cryo-X-ray diffraction (XRD) was performed on commercial Li powders. As shown in Figure 4c, two XRD patterns recorded at 300 and 100 K are quite similar. The slight peak shift to high angles demonstrate a tiny volume shrinkage due to the cooled-down atomic thermal motion when the temperature dropped from 300 to 100 K, resulting in the reduction of the lattice *a* value from 3.51 to 3.48 Å, consistent with the previous reports.[27,28] In addition, the 100 K temperature in this work is not low enough to cause Li metal-phase transformation from cubic phase to hexagonal phase (below 80 K).[27,28] Therefore, the cryo-XRD results suggest a negligible effect of low temperature (100 K < T < 300 K) on the Li metal structure. The results from the cryo-TEM are the true reflection of the EDLi dominated by the electrochemical process. The EDLi is astonishingly amorphous in the first 5 min deposition at 0.5 mA cm^{-2}, which is led by the nucleation. Similar to the quenching, the instant large overpotential (about −220 mV in Figure S1a) in the cell is believed to result in the glassy (noncrystalline) EDLi at the beginning. The EDLi will crystallize after long-term deposition (for example, 2 h plating), as demonstrated in Figure S5 with some characteristic metallic Li bright spots. The transformation

DOI: 10.1021/acs.nanolett.7b03606
Nano Lett. XXXX, XXX, XXX−XXX

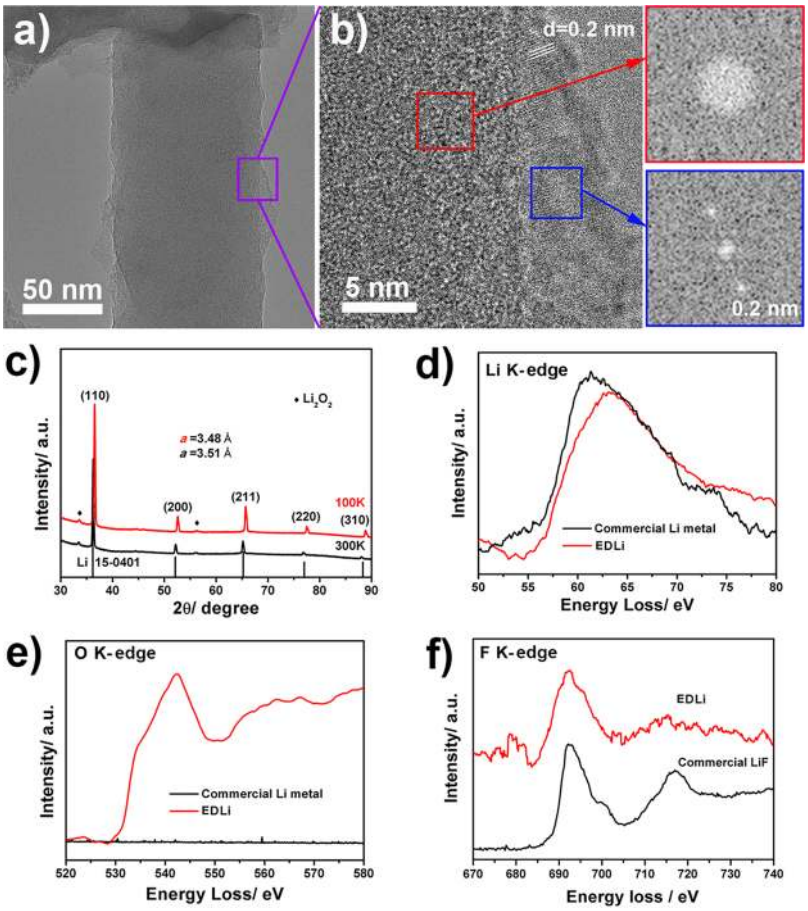

Figure 4. Cryo-TEM (a) image and (b) its regional zoomed-in image with the bulk and surface FFT result of the EDLi using conventional carbonate electrolyte. (c) XRD comparison of the commercial Li metal powder at 300 and 100 K. EELS spectra comparison of the reference (commercial Li ribbon and LiF) to the EDLi in (d) Li K-edge, (e) O K-edge, and (f) F K-edge.

from amorphous to crystalline EDLi will be explored in the future.

Electron energy loss spectroscopy (EELS) was used to elucidate the chemical information on the EDLi. Commercial Li metal ribbon was scrapped onto the Cu grid in the glovebox filled with argon (schematic process shown in Figure S6) and tested in the same condition as the EDLi for reference. The absence of a peak in the O K-edge EELS spectrum (Figure 4e) shows no significant Li metal oxidation, indicating that the transfer process avoids air exposure. In the Li K-edge spectrum (Figure 4d), the pure metallic Li shows a weak pre-peak centered at 55 eV and a major broad peak centered at 62 eV. The Li K-edge spectrum of the EDLi (pre-peak at 56 eV and a major broad peak at 63 eV) compared to the reference spectrum (Figure 4d), which implies that the EDLi is indeed metallic. The slight peak shift is attributed to the amorphous nature of the EDLi surrounded by the SEI, while the reference Li is crystalline without any surface contamination. The presence of the SEI on the EDLi is validated by the O K-edge (Figure 4e), F K-edge (Figure 4f), and C K-edge (Figure S7) spectra. Further analysis of the spectra indicates that the SEI consists of inorganic species (e.g., LiF, Li_2O, and Li_2CO_3) and organic species (e.g., esters, ethers, and carboxylates), in line with the previous reports.[29] Overall, the EDLi is metallic transformed from initial amorphous structure. The SEI unevenly covers the Li metal surface and contains some crystalline LiF. However, with such nanostructure, the CE of the cell using conventional carbonate electrolyte is 60% at the first cycle (Figure S8), which is too low for practical use, causing the rapid cell failure.

Influence of Metal-Ion Electrolyte Additives. To increase the CE, some functional additives have been added to the electrolytes and show positive effects on improving the reversibility of the Li metal.[30,31] One group of the additives is the metal ions, which can be further categorized into alloyed species (e.g., Mg^{2+}, Zn^{2+}, and Al^{3+} etc.)[31−34] and nonalloyed species (e.g., Cs^+ and Rb^+)[35,36] according to their reactivity with Li. The former is believed to protect the Li metal with intermediated alloyed phases. The latter is designed to remain as free charged ions that guide the deposition of Li metal by electrostatic interaction. However, these two mechanisms have not been confirmed at the nanoscale. Therefore, taking Cs^+ and Zn^{2+} additives as examples, their influences on the nanostructures of the EDLi were explored to deepen the understanding of their underlying mechanisms.

As expected, the CE of the cells improved when Cs^+ (86% at the first cycle, Figure S8) and Zn^{2+} (89% at the first cycle, Figure S8) were added to the conventional electrolyte. SEM images (Figure S9) show a similar obtained ribbon morphology from three electrolytes (pristine, Cs^+ and Zn^{2+} containing electrolytes) with different complexity. Clearly, the additives form dense interwoven Li films (Figure S9). In particular, Cs^+ facilitates the Li metal to grow vertically and form aligned arrays, consistent with the work conducted by Zhang and co-

DOI: 10.1021/acs.nanolett.7b03606
Nano Lett. XXXX, XXX, XXX−XXX

workers.[37] The smooth Li deposition in the Cs^+-containing electrolyte is proposed to be the result of a synergistic effect of the Cs^+ additive and LiF-rich thick SEI, which results from the decomposition of $CsPF_6$ at 2.05 V.[37] The cryo-TEM results (Figure 5a–c) exhibit that the Li metal plated from Cs^+-containing electrolyte has a dense, uniform and ultrathin SEI (<1 nm) on the surface, which is similar to that of the SEI formed on graphite anode surface in the $CsPF_6$-containing electrolyte reported by Xiang et al.,[38] demonstrating the positive effect of Cs^+ additive on the SEI formation. However, a conformal thick surface film was found along the surface of the Li metal when the cell was cycled with Zn^{2+} containing electrolyte (Figure 5d). The surface is rough and about 10 nm in average thickness. As discussed before, the EDLi is consistently amorphous in the bulk with a partially crystallized SEI, determined to be composed of LiF given characteristic bright spots (Figure 5f). Furthermore, the Li–Zn alloy is also amorphous without any of the characteristic bright rings and spots present in Figure 5e and 5f. Note that the Zn^{2+} containing electrolyte has a higher CE and thicker surface layer than that of the pristine electrolyte. The Li–Zn alloy is believed to be distributed on the surface and protect the Li metal from electrolyte corrosion. Overall, both of the EDLi from Cs^+- and Zn^{2+}-containing electrolytes are amorphous, suggesting there is little effect on the Li bulk structure; however, they differ significantly in their interfacial properties.

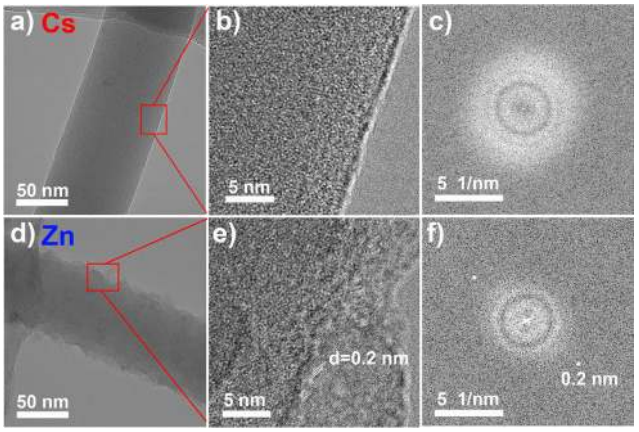

Figure 5. Cryo-TEM images (a, b, d, e) with their corresponding area FFT analysis (c, f) of the deposited Li metal using electrolytes containing (a–c) Cs^+ and (d–f) Zn^{2+} additives at 400 000× magnification.

The above observations were further confirmed by the surface sensitive XPS, obtaining the chemical compositions of the SEI. The presence of Cu signal in the survey spectra (Figure 6a) and metallic Li in the Li 1s spectra (Figure 6b) indicates an ultrathin surface film from the Cs^+-containing electrolyte, consistent with the SEI measured by cryo-TEM (Figure 5a,b). Figure 6a,c demonstrate fewer fluorine species in Cs^+ than in Zn^{2+} containing electrolyte, which could be due to the thinner SEI film thickness formed in Cs^+-containing electrolyte. The SEI from all electrolytes is composed of inorganic compounds (e.g., LiF, Li_2O, and Li_2CO_3 in Figure 6c) and organic species (e.g., esters, ethers, and carboxylates in Figure 6d). Some oxygenated fluorines ($Li_xPO_yF_z$)[39,40] were observed when the Cs^+ and Zn^{2+} were added in the electrolyte (Figure 6c). In addition, both ions are found to be partially reduced because there is a weak signal from metallic Cs (Figure 6e) and a strong signal from metallic Zn (Figure 6f). The latter confirms the presence of Li-Zn alloy on the surface of the EDLi.

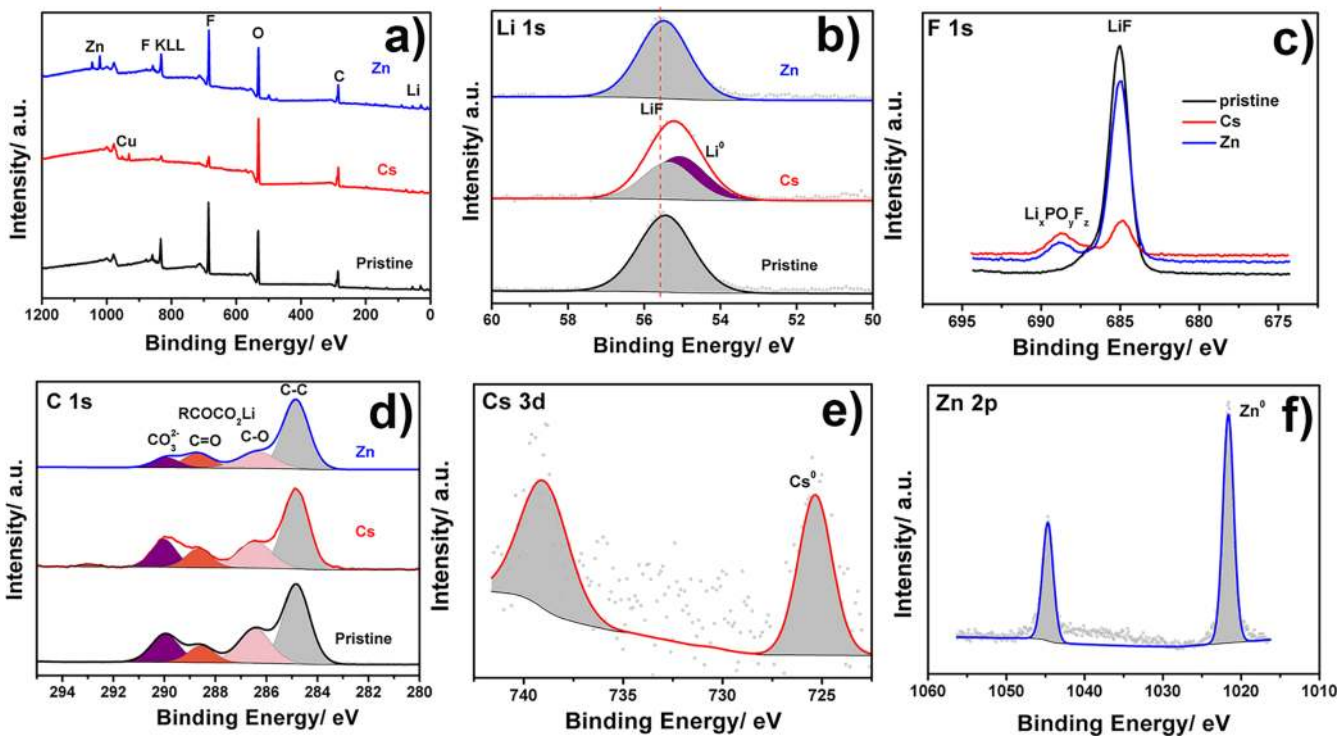

Figure 6. Comparison of (a) XPS spectra of the survey, (b) C 1s, (c) F 1s, (d) Li 1s, (e) Cs 3d, and (f) Zn 2p with the deposited Li metal from the pristine Cs^+ and Zn^{2+} containing electrolytes.

DOI: 10.1021/acs.nanolett.7b03606
Nano Lett. XXXX, XXX, XXX–XXX

As shown above, three different electrolytes give rise to three distinctive surface properties on the EDLi, especially in the spatial distribution and composition of the SEI. (1) Coverage: The SEI partially covered the EDLi from the pristine electrolyte, while it fully covered the EDLis from the Cs^+ and Zn^{2+} ions containing electrolytes. Considering their CE difference, the fully covered SEI is beneficial to achieve the high CE. (2) Composition: The SEI is a combination of the inorganic components (e.g., LiF, Li_2O, Li_2CO_3, and $Li_xPO_yF_z$) and organic species (e.g., esters, ethers and carboxylates). A good SEI should be robust and ionic-conductive yet electrically insulated, which requires to adjust the component species, crystallinity, and spatial distribution meanwhile. Take the LiF as an example; the previous experimental results showed that the CE increased when the LiF was added into the electrolyte.[41] However, the LiF in the SEI is found to be crystalline in this work, which has a very low ionic conductivity ($<10^{-12}$ S cm^{-1}).[42,43] In this regard, the functioning mechanism of the LiF should be doubted, but compounds such as $Li_xPO_yF_z$ need to be taken into account because the amorphous $Li_xPO_yF_z$ may have a higher ionic conductivity than the crystalline LiF, which will contribute to increasing the CE. (3) Relationship between CE and SEI: Although ultrathin (<1 nm) and thick (~10 nm) SEIs were observed for the Cs^+- and Zn^{2+}-containing electrolytes, they showed comparable CE in the beginning, which indicates that the CE is not proportional to the SEI content. The reaction between EDLi and electrolyte consumes the metallic Li. This is the irreversible chemical source depending on the nanostructure of the EDLi. Another source is the "dead" Li physically isolated from the conductive network, which relies on the micro architecture of the EDLi. In this regard, the one-dimensional network from the Cs^+ containing electrolyte seems as good as the three-dimensional network formed in the Zn^{2+} containing electrolyte. Therefore, to achieve high CE, both the nanostructure and micro-architecture of the EDLi should be taken into account. This requires researchers to optimize the electrolytes and substrates in the meantime.

In summary, a new cryogenic electron microcopy method was developed to probe the nanostructure and chemical composition of the electrochemically deposited Li metal (EDLi) while minimizing beam damage. The short plating time (5 min at 0.5 mA cm^{-2}) of Li metal in the conventional electrolyte (1 M $LiPF_6$ in EC/EMC) is amorphous Li with an uneven SEI distributed on its surface and consisted of the amorphous organic species and crystalline LiF. The surface property of the EDLi can be adjusted by adding the functional metal ions to the electrolytes, which results in the distinctive SEI and increases slightly the CE during electrochemical cycling. Further comparison confirms the importance of a fully covered surface film. Based on the current observation, the positive effect of LiF is questioned, and the relationship between SEI and CE is reconsidered. Our methodology demonstrates that cryo-TEM is a powerful tool that can be used to characterize beam(thermal)-sensitive battery materials, especially for the fragile cycled electrode materials. The cryotechnique stabilizes the samples against a continuous E-beam and provides real information dominated by the electrochemical process. These results deliver fundamental understanding of structure information on the electrochemically deposited Li metal. By means of the cryo-TEM, we will be able to clarify the influences of the various factors such as different electrolyte salts, solvents, additives, and concentration on the nanoscale structure of the deposited Li metal in the future. These new insights can lead the battery community to propose more-effective optimization strategies to make the Li metal a practical anode.

■ ASSOCIATED CONTENT

Supporting Information

The Supporting Information is available free of charge on the ACS Publications website at DOI: 10.1021/acs.nanolett.7b03606.

Additional details on supplementary methods; experimental setups; structural information on Li and LiF; and additional SEM, TEM, EELS, and electrochemical tests. (PDF)

■ AUTHOR INFORMATION

Corresponding Author

*E-mail: shirleymeng@ucsd.edu.

ORCID

Xuefeng Wang: 0000-0001-9666-8942
Wu Xu: 0000-0002-2685-8684
Ji-Guang Zhang: 0000-0001-7343-4609
Jun Liu: 0000-0001-8663-7771
Ying Shirley Meng: 0000-0001-8936-8845

Author Contributions

X.W. and Y.M. conceived the idea. X.W. designed the experiments and conducted most of the characterizations. X.W., M.Z., S.W., and J.B. performed the TEM and analyzed the data. All authors discussed the results and commented on the manuscript. The manuscript was written through the contributions of all authors. All authors have given approval to the final version of the manuscript.

Funding

This work was supported by the Assistant Secretary for Energy Efficiency and Renewable Energy, Office of Vehicle Technologies of the U.S. Department of Energy under the Battery500 consortium. Partial funding for the development of cryogenic technique is provided by Assistant Secretary for Energy Efficiency and Renewable Energy, Office of Vehicle Technologies of the U.S. Department of Energy (DOE) under contract no. DE-AC02-05CH11231, subcontract no. 7073923, under the Advanced Battery Materials Research (BMR) Program.

Notes

The authors declare no competing financial interest.

■ ACKNOWLEDGMENTS

We acknowledge the use of the University of California San Diego Cryo-Electron Microscopy Facility, which is supported by NIH grants to T.S.B. and a gift from the Agouron Institute to UCSD. The SEM was performed in part at the San Diego Nanotechnology Infrastructure (SDNI), a member of the National Nanotechnology Coordinated Infrastructure, which is supported by the National Science Foundation (grant no. ECCS-1542148). XPS work was performed at the UC Irvine Materials Research Institute (IMRI) using instrumentation funded in part by the National Science Foundation Major Research Instrumentation Program under grant no. CHE-1338173. We thank Dr. Bao Qiu for assistance in schematic drawing.

DOI: 10.1021/acs.nanolett.7b03606
Nano Lett. XXXX, XXX, XXX−XXX

ABBREVIATIONS

EDLi, electrochemical deposited Li metal
SEI, solid electrolyte interphase
CE, Coulombic efficiency
TEM, transmission electron microscopy

REFERENCES

(1) Xu, W.; Wang, J. L.; Ding, F.; Chen, X. L.; Nasybulin, E.; Zhang, Y. H.; Zhang, J. G. *Energy Environ. Sci.* **2014**, *7* (2), 513−537.
(2) Lin, D.; Liu, Y.; Cui, Y. *Nat. Nanotechnol.* **2017**, *12* (3), 194−206.
(3) WHITTINGHAM, M. S. *Science* **1976**, *192* (4244), 1126−1127.
(4) Aurbach, D.; Zinigrad, E.; Cohen, Y.; Teller, H. *Solid State Ionics* **2002**, *148* (3−4), 405−416.
(5) Etacheri, V.; Marom, R.; Elazari, R.; Salitra, G.; Aurbach, D. *Energy Environ. Sci.* **2011**, *4* (9), 3243−3262.
(6) Bruce, P. G.; Freunberger, S. A.; Hardwick, L. J.; Tarascon, J. M. *Nat. Mater.* **2011**, *11* (1), 19−29.
(7) Cheng, X.-B.; Zhang, R.; Zhao, C.-Z.; Wei, F.; Zhang, J.-G.; Zhang, Q. *Advanced Science* **2016**, *3* (3), 1500213.
(8) Zheng, J.; Engelhard, M. H.; Mei, D.; Jiao, S.; Polzin, B. J.; Zhang, J.-G.; Xu, W. *Nature Energy* **2017**, *2*, 17012.
(9) Zhang, X.-Q.; Cheng, X.-B.; Chen, X.; Yan, C.; Zhang, Q. *Adv. Funct. Mater.* **2017**, *27* (10), 1605989.
(10) Qian, J.; Henderson, W. A.; Xu, W.; Bhattacharya, P.; Engelhard, M.; Borodin, O.; Zhang, J. G. *Nat. Commun.* **2015**, *6*, 6362.
(11) Lu, Y. Y.; Tikekar, M.; Mohanty, R.; Hendrickson, K.; Ma, L.; Archer, L. A. *Adv. Energy Mater.* **2015**, *5* (9), 1402073−1402080.
(12) Steiger, J.; Kramer, D.; Mönig, R. *J. Power Sources* **2014**, *261*, 112−119.
(13) Wood, K. N.; Kazyak, E.; Chadwick, A. F.; Chen, K.-H.; Zhang, J.-G.; Thornton, K.; Dasgupta, N. P. *ACS Cent. Sci.* **2016**, *2* (11), 790−801.
(14) Chang, H. J.; Trease, N. M.; Ilott, A. J.; Zeng, D.; Du, L.-S.; Jerschow, A.; Grey, C. P. *J. Phys. Chem. C* **2015**, *119* (29), 16443−16451.
(15) Cohen, Y. S.; Cohen, Y.; Aurbach, D. *J. Phys. Chem. B* **2000**, *104* (51), 12282−12291.
(16) Mogi, R.; Inaba, M.; Iriyama, Y.; Abe, T.; Ogumi, Z. *J. Electrochem. Soc.* **2002**, *149* (4), A385−A390.
(17) Nie, M.; Demeaux, J.; Young, B. T.; Heskett, D. R.; Chen, Y.; Bose, A.; Woicik, J. C.; Lucht, B. L. *J. Electrochem. Soc.* **2015**, *162* (13), A7008−A7014.
(18) Nie, M.; Lucht, B. L. *J. Electrochem. Soc.* **2014**, *161* (6), A1001−A1006.
(19) Taylor, K. A.; Glaeser, R. M. *Science* **1974**, *186* (4168), 1036−1037.
(20) Sirohi, D.; Chen, Z.; Sun, L.; Klose, T.; Pierson, T. C.; Rossmann, M. G.; Kuhn, R. J. *Science* **2016**, *352* (6284), 467−470.
(21) Bartesaghi, A.; Merk, A.; Banerjee, S.; Matthies, D.; Wu, X.; Milne, J. L. S.; Subramaniam, S. *Science* **2015**, *348* (6239), 1147−1151.
(22) Nogales, E. *Nat. Methods* **2015**, *13* (1), 24−27.
(23) Li, X.; Mooney, P.; Zheng, S.; Booth, C. R.; Braunfeld, M. B.; Gubbens, S.; Agard, D. A.; Cheng, Y. *Nat. Methods* **2013**, *10* (6), 584−590.
(24) Milazzo, A.-C.; Moldovan, G.; Lanman, J.; Jin, L.; Bouwer, J. C.; Klienfelder, S.; Peltier, S. T.; Ellisman, M. H.; Kirkland, A. I.; Xuong, N.-H. *Ultramicroscopy* **2010**, *110* (7), 741−744.
(25) Li, S.; Bouwer, J.; Duttweiler, F.; Ellisman, M.; Jin, L.; Leblanc, P.; Milazzo, A.; Peltier, S.; Xuong, N.; Kleinfelder, S. *A New Direct Detection Camera System for Electron Microscopy*; International Society for Optics and Photonics: Bellingham, WA, 2008; pp 6068001−60680010.
(26) Chattopadhyay, S.; Lipson, A. L.; Karmel, H. J.; Emery, J. D.; Fister, T. T.; Fenter, P. A.; Hersam, M. C.; Bedzyk, M. J. *Chem. Mater.* **2012**, *24* (15), 3038−3043.
(27) McCarthy, C. M.; Tompson, C. W.; Werner, S. A. *Phys. Rev. B: Condens. Matter Mater. Phys.* **1980**, *22* (2), 574−580.
(28) Berliner, R.; Werner, S. A. *Physica BC* **1986**, *136* (1), 481−484.
(29) Sina, M.; Alvarado, J.; Shobukawa, H.; Alexander, C.; Manichev, V.; Feldman, L.; Gustafsson, T.; Stevenson, K. J.; Meng, Y. S. *Adv. Mater. Interfaces* **2016**, *3* (20), 1600438.
(30) Qian, J.; Xu, W.; Bhattacharya, P.; Engelhard, M.; Henderson, W. A.; Zhang, Y.; Zhang, J.-G. *Nano Energy* **2015**, *15*, 135−144.
(31) Haregewoin, A. M.; Wotango, A. S.; Hwang, B. J. *Energy Environ. Sci.* **2016**, *9* (6), 1955−1988.
(32) Ishikawa, M.; Machino, S.-i.; Morita, M. *J. Electroanal. Chem.* **1999**, *473* (1−2), 279−284.
(33) Matsuda, Y.; Ishikawa, M.; Yoshitake, S.; Morita, M. *J. Power Sources* **1995**, *54* (2), 301−305.
(34) Matsuda, Y. *J. Power Sources* **1993**, *43* (1), 1−7.
(35) Kim, J.-S.; Kim, D. W.; Jung, H. T.; Choi, J. W. *Chem. Mater.* **2015**, *27* (8), 2780−2787.
(36) Ding, F.; Xu, W.; Graff, G. L.; Zhang, J.; Sushko, M.; Chen, X.; Shao, Y.; Engelhard, M. H.; Nie, Z.; Xiao, J.; Liu, X.; Sushko, P. V.; Liu, J.; Zhang, J.-G. *J. Am. Chem. Soc.* **2013**, *135* (11), 4450−4456.
(37) Zhang, Y.; Qian, J.; Xu, W.; Russell, S. M.; Chen, X.; Nasybulin, E.; Bhattacharya, P.; Engelhard, M. H.; Mei, D.; Cao, R.; Ding, F.; Cresce, A. V.; Xu, K.; Zhang, J. G. *Nano Lett.* **2014**, *14* (12), 6889−6896.
(38) Xiang, H.; Mei, D.; Yan, P.; Bhattacharya, P.; Burton, S. D.; von Wald Cresce, A.; Cao, R.; Engelhard, M. H.; Bowden, M. E.; Zhu, Z.; Polzin, B. J.; Wang, C.-M.; Xu, K.; Zhang, J.-G.; Xu, W. *ACS Appl. Mater. Interfaces* **2015**, *7* (37), 20687−20695.
(39) Ensling, D.; Stjerndahl, M.; Nyten, A.; Gustafsson, T.; Thomas, J. O. *J. Mater. Chem.* **2009**, *19* (1), 82−88.
(40) Schroder, K. W.; Celio, H.; Webb, L. J.; Stevenson, K. J. *J. Phys. Chem. C* **2012**, *116* (37), 19737−19747.
(41) Lu, Y.; Tu, Z.; Archer, L. A. *Nat. Mater.* **2014**, *13* (10), 961−969.
(42) Geschwind, G. *J. Phys. Chem. Solids* **1969**, *30* (6), 1631−1635.
(43) Pan, J.; Cheng, Y.-T.; Qi, Y. *Phys. Rev. B: Condens. Matter Mater. Phys.* **2015**, *91* (13), 134116.

NOTE ADDED AFTER ASAP PUBLICATION

This paper published ASAP on 11/2/2017. Several additional changes were made and the revised version reposted on 11/3/2017.

DOI: 10.1021/acs.nanolett.7b03606
Nano Lett. XXXX, XXX, XXX−XXX